HHS Public Access

Structural Analysis of Ion Selectivity in the NaK Channel

Amer Alam[1] and **Youxing Jiang**[1,2]

[1]Department of Physiology, University of Texas Southwestern Medical Center, 5323 Harry Hines Blvd., Dallas, Texas Dallas, Texas 75390-9040

[2]Howard Hughes Medical Institute, 5901 Forest Park Drive, Dallas, TX 75390-9050

Abstract

Here, we present a detailed characterization of ion binding in the NaK pore using the high resolution structures of NaK in complex with various cations. These structures reveal four ion binding sites with similar chemical environments but vastly different ion preference. The most non selective of all is site 3, which is formed exclusively by backbone carbonyl oxygen atoms and resides deep within the selectivity filter. Additionally, four water molecules in combination with four backbone carbonyl oxygen atoms are seen to participate in K^+ and Rb^+ ion chelation both at the external entrance and vestibule of the NaK filter, confirming the preference for an octahedral ligand configuration for K^+ and Rb^+ binding. In contrast, Na^+ binding in the NaK filter, particularly at site 4, utilizes a pyramidal ligand configuration requiring the participation of a water molecule in the cavity. Therefore, the ability of the NaK filter to bind both Na^+ and K^+ ions seemingly arises from the ions' ability to utilize the existing environment in unique ways rather than any structural rearrangements of the filter itself.

Along with channel gating, the ability of ion channels to select for and allow the passage of specific ions through their conduction pores is central to their physiological functioning [1]. Our knowledge of ion selectivity, as this process is known, has come a long way with the determination of several K^+ selective ion channel structures over the past decade [2-7]. However, several fundamental issues are yet to be fully understood and remain the focus of ongoing debate within the field. For example, is the snug-fit model alone enough to account for K^+ over Na^+ selectivity or do ligand chemical environment (eight carbonyl oxygen atoms) and dynamics play the determinant role [8, 9]?

The recently discovered NaK channel from *B. cereus* has provided a unique structural model for further probing mechanisms of ion selectivity. The channel shares overall structural similarities with KcsA but has been shown to conduct most group 1A cations as well as Ca^{2+}, using a unique mode of Ca^{2+} chelation with only backbone carbonyl oxygen atoms acting as ligands [10, 11]. This ion non-selectivity is thought to arise from structural

differences within the selectivity filter, where only the two most intracellular K^+ binding sites of KcsA (sites 3 and 4) are preserved while the upper two are replaced by a vestibular structure. Using the initial NaK structure, an analysis of structural differences among complexes of NaK and its various conducting ions has been difficult due to resolution limits as well as the presence of a high Ca^{2+} concentration in addition to monovalent cations in crystallization solutions. To decipher the underlying mechanisms by which various monovalent cations are able to permeate NaK, we crystallized a truncated form of the channel, NaKN 19, previously used for channel function analysis. Well diffracting crystals were obtained and the structures were determined at resolutions ranging from 1.6 – 2.0 Å, revealing a channel in an open conformation. A detailed analysis of gating mechanics was carried out and is presented in our companion study. Here we use the high resolution structures of NaKN 19 in complex with various mono- and divalent cations to visualize the differences in ion binding profiles among various conducting ions at atomic detail. While our structural study reveals ion binding profiles in the NaK filter at atomic detail and reveals several interesting features that underlie NaK ion non-selectivity, fundamental questions remain about how sites with seemingly identical chemical environments can display different ion binding properties.

Results

Na+ binding in NaK selectivity filter

The structure of the NaKN 19-Na^+ complex was determined at 1.8 Å resolution and its $2F_o$-F_c ion omit map reveals three bound ions in the selectivity filter: in the vestibule, and sites 3 and 4 (Fig. 1a). The density in the vestibule and site 4 can be assigned to Na^+ ions but that at site 3 cannot, as will be discussed in detail later. The ion in the vestibule is coordinated by four carbonyl oxygen atoms of Val64s with a ligand-ion distance of about 2.9 Å. Four water molecules are clearly seen to reside within the vestibule, each with a distance of about 4 Å to the Na^+ ion, suggesting no intimate interaction between the ion and the water molecules. The Na^+ ion in site 4 does not reside in the center of the ion binding cage formed by the hydroxyl and backbone carbonyl oxygen atoms from Thr63. Instead it sits in an almost planar conformation with respect to its ligands, namely the four hydroxyl oxygen atoms of Thr63s, with a distance of 2.4 Å. Furthermore, another water molecule in the central cavity, only seen in the Na^+ complex, also participates in Na^+ coordination with a Na^+-O distance of 2.7 Å. This scheme of pyramidal Na^+ coordination is reminiscent of what is seen in the Na^+ complex of the Guanine tetraplex structure [12], part of which is shown in figure 1b, drawn based on a 0.95 Å crystal structure of the complex. By using the O6 of the guanine base, the Guanine tetraplex generates a set of Na^+ binding sites that have a similar chemical environment as in NaK and K^+ channels (Supplementary fig 1). Na^+ ions have a versatile way of binding and the one near the 3′ end is planar with the tetrad and has a water molecule axial to it (fig. 1b). The distances between Na^+ and O6 or water are in the range of 2.32 – 2.4 Å.

Identification of the bound ion at site 3 was complicated due to its apparent contamination by an unknown heavy atom ion or a mixture of ions. Even though 100 mM NaCl was the only salt present in crystallization conditions, electron density at site 3 is too strong to be

accounted for solely by Na^+ ions. The bound ion also carries an anomalous signal as shown in the anomalous difference Fourier map (Supplementary fig. 2a). We suspect the source of this contamination is $(\pm)$-2-Methyl-2,4-pentanediol (MPD), used as a precipitant at high concentrations in the crystallization of NaKN 19 (Methods). MPD treatment with chelating resins carrying moieties for non-selective binding of both monovalent and divalent heavy metal ions can decrease the extent of contamination but, unfortunately, not eliminate it. Contamination from trace metal ions is not surprising judging from the very non selective nature of site 3, as will be discussed in further detail later. For simplicity, in our structural analysis we have assigned this strong density to Cs^+ and refined its occupancy to reveal the extent of the contamination. Even though the contamination obscures a direct visualization of possible Na^+ binding at site 3, important information can still be extracted from an analysis of electron density distribution. A $F_{low\ Na}$-$F_{high\ Na}$ difference map between NaKN 19 crystals grown in 100 mM NaCl (low Na) and those grown in 500 mM NaCl (high Na) reveals a strong peak at site 3, indicating the replacement of some contaminating heavy atoms by the less electron dense Na^+ ions (Supplementary fig. 2b). This is also evident from a decrease in ion occupancy of the heavy atoms (Cs^+ for the purpose of refinement) in the High Na^+ crystals. We therefore conclude that Na^+ does indeed bind at site 3 albeit at low affinity. Recent computational studies have suggested that Na^+ ions tend to bind at the upper or lower ends of the ion binding cage at site 3, almost planar with the backbone carbonyls of Val64 or Thr63 [13, 14]. Three observations from NaKN 19 structures lead us to believe this is actually the case. First, the football shaped electron density at site 3 in a $2F_o$-F_c ion omit map (Fig. 1c upper) indicates the presence of weak scattering elements at both end of the site. Second, a F_o-F_c difference map of the high Na^+ crystal reveals unaccounted density on both ends of the site that likely comes from bound Na^+ ions (Fig. 1c, lower). This density is weak (4 sigma in figure 1c), as would be expected from a low occupancy and low scattering power of Na^+ ions. Finally, a similar planar conformation of a Na^+ ion with its ligand is observed at site 4. Thus, 3 distinct Na^+ binding positions are likely formed by sites 3 and 4 where the ions can be chelated in plane with their ligands (Fig. 1d), and the observed electron density in the filter is the combined effect of the ion distribution shown in figure 1 a&d.

K^+ & Rb^+ complex structures of NaKN 19

K^+- and Rb^+-complex structures of NaKN 19 were determined at 1.8 Å and 1.7 Å, respectively. While ion binding in the NaK filter is similar between both complexes, the details governing their ion chelation properties are noticeably different from the Na^+-complex. Both K^+ and Rb^+ display a strong preference for maintaining an octahedral arrangement of ligands. Figure 2 shows a $2F_o$-F_c ion omit map of the K^+(a) and Rb^+ (b) complex of NaKN 19, revealing four ion binding sites: the external entrance, vestibule, and sites 3 & 4. While no Na^+ binding was observed at the external entrance, K^+ and Rb^+ bind there in a partially hydrated manner with the four carbonyl oxygen atoms from the Gly67 residues and four water molecules acting as ligands. A partially hydrated K^+ ion at a similar position has been observed in the KcsA structure[15]. However, the carbonyl oxygen atoms of Gly67, rather than pointing upwards as in KcsA, are oriented more inward, forming a better chelation scheme for K^+ and Rb^+. Partially hydrated K^+ and Rb^+ ions are also observed in the vestibule of the filter chelated by the four carbonyl oxygen atoms of Val64s

along with 4 water molecules. Thus, the involvement of water molecules allows for the maintenance of an octahedral ligand arrangement (Fig. 2c), much like that seen in KcsA [15]. It is important to note that these four water molecules are also seen within the vestibule of the filter in the Na^+ complex but, with ion-ligand distances of ~ 4 Å, are unlikely to be involved in ion chelation. K^+ and Rb^+ binding at sites 3 and 4 is virtually the same as that at equivalent sites in K^+ channels both in terms of position and ligand coordination. Heavy atom contamination at site 3 was still observed in the K^+ and Rb^+ complexes, but to a much lesser extent than in the Na^+ complex based on the following observation. A $F_{Na} - F_K$ difference map between crystals grown in 100 mM NaCl and KCl reveals strong electron density peak at site 3 (Supplementary fig. 3), despite K being a stronger X-ray scattering element than Na. This alludes to a competitive knockout of a larger fraction of the contaminating ion/ions by K^+, akin to a $F_{heavy}-F_K$ map. This suggests that K^+ binds at site 3 better than Na^+. Taken together with the observation of K^+ binding at the external entrance, along with the functional observation that K^+ has a larger effect on reducing ^{86}Rb influx into liposomes compared to Na^+ [11], it is reasonable to conclude that NaK is more selective for K^+ than Na^+.

Analysis of Cs$^+$ binding in NaK filter

Our analysis of monovalent cation binding in NaK was also extended to the larger Cs^+ ions. Even though we failed to produce crystals of NaKN 19 grown in 100 mM CsCl, the structure of a K^+ complex of NaKN 19 soaked in a stabilization solution containing 67 mM KCl and 33 mM CsCl (Methods) was determined at 1.8 Å resolution. The $F_{Cs\ soak} - F_K$ difference map between this soaked crystal and the native K^+ complex crystal revealed a strong peak at site 3 (Fig. 2d). No K^+ replacement by Cs^+ was observed at the external entrance or site 4, indicating that Cs^+ appears to have a strong preference for site 3 with no detectable binding at the extracellular entrance and site 4 in the presence of K^+.

Divalent cation binding in the NaK filter

Although we were unable to crystallize NaKN 19 in $CaCl_2$ alone, we co-crystallized NaKN 19 in the presence of $CaCl_2$ in addition to 100 mM NaCl. In the presence of 10 mM Ca^{2+}, clear density observed at the external entrance in a $2F_o$-F_c ion omit map (Fig. 3a) which, considering no obvious Na^+ binding at this site, can be attributed to Ca^{2+} binding. To probe the binding affinity of Ca^{2+} at this site, we performed a crystallographic titration assay by obtaining NaKN 19 crystals at different Ca^{2+} concentrations (0.5, 1.0, 2.5, 5.0 and 10 mM). Figure 3b shows two examples of the resulting difference maps between crystals with and without Ca^{2+} ($F_{0.5mM\ Ca^{2+}} - F_{0mM\ Ca^{2+}}$ and $F_{5mM\ Ca^{2+}} - F_{0mM\ Ca^{2+}}$), revealing stronger electron density from bound Ca^{2+} at the external site at higher $[Ca^{2+}]$. Since the only variable in crystallization conditions from which all crystals were obtained was the Ca^{2+} concentration and all diffraction data were scaled against that of the same native crystal, the difference in intensity of the electron density at the external entrance reflects the extent of Ca^{2+} binding, or occupancy, at the external site. Figure 3c shows a one-dimensional electron density profile corresponding to Ca^{2+} binding at the external entrance plotted along the central axis of the filter (Methods). An increase in Ca^{2+} occupancy is clearly seen with increasing Ca^{2+} concentrations. Crystals grown in 5 and 10 mM Ca^{2+} display a similar intensity of electron density, pointing to a saturation of Ca^{2+} binding at

10mM. This can be further verified by refining Ca^{2+} occupancy of the NaKN 19 co-crystallized with 10 mM Ca^{2+}, which gives rise to a value of 0.99. Assuming a spherical distribution of electron density from the bound Ca^{2+}, the integration of the area under each peak of the 1-D electron density profile and plotting these values against Ca^{2+} concentration (Fig. 3d) yields a K_d of 1.8 mM for the external site at pH 7.5 and in the presence of 100 mM Na^+, conditions under which the associated crystals were obtained. Ca^{2+} has also been shown to bind site 3 previously [10]. However its affinity cannot be determined by a similar titration assay because of competition from Na^+ and trace element binding at this site. Nevertheless Ca^{2+} binding at site 3 can be further confirmed by analyzing the effect of increasing Ca^{2+} concentration on the electron density profile at site 3. It is clear that increasing Ca^{2+} concentrations cause a corresponding decrease in electron density at this site, indicated by stronger peaks in the $F_{0\ Ca}{}^{2+}$-$F_{+\ Ca}{}^{2+}$ difference maps (supplementary fig. 4). This points to an increase in the replacement of contaminating heavy atom by the lighter Ca^{2+} ions upon increasing Ca^{2+} concentrations.

Attempts at crystallizing NaKN 19 in the presence of Ba^{2+} also failed to yield high quality crystals. Consequently, we soaked a crystal of the K^+-complex of NaKN 19 in a stabilization solution containing 67 mM KCl and 33 mM $BaCl_2$ (Methods) to analyze Ba^{2+} binding and determined its structure at 2.0 Å resolution. The $F_{Ba^{2+}\ soak} - F_K$ difference map between the Ba^{2+} soaked crystal and the native K^+ complex crystal confirms two Ba^{2+} binding positions, the external entrance and site 3, as was observed before[11] (Fig. 4a). Even though Ba^{2+} is present at half the concentration of K^+, refinement of the ion at the external site as Ba^{2+} in the soaked crystal gives rise to an occupancy of 0.97. This indicates an almost complete replacement of K^+ at the external site, suggesting a higher affinity for Ba^{2+} than K^+. Ba^{2+} coordination at the external site is similar to that of K^+ and Rb^+, with 4 water molecules and 4 carbonyl oxygen atoms of Gly67s serving as the 8 ligands (Fig. 4b). This is different from Ca^{2+} binding, where no hydration shell was observed in external Ca^{2+} chelation (fig. 3a). This does not necessary mean that water molecules do not participate in external Ca^{2+} chelation. It could simply be that because Ca^{2+} prefers 6 or 7 ligands as in other Ca^{2+} binding motifs like the EF-hand [16-18], the symmetry mismatch between the channel and the configuration of Ca^{2+} chelation leads to a 4-fold reduction in occupancy of the water molecules. It is also interesting to note that even though sites 3 & 4 in KcsA have a virtually identical chemical environment as the corresponding sites in NaK, Ba^{2+} only binds at the external entrance and site 3 in NaK instead of sites 2 and 4 as in KcsA [19, 20].

Although we were unable to carry out an analysis of Ba^{2+} affinity at both sites, we expect it to be fairly high for at least one of them based on results from ^{86}Rb flux assays. Figure 4c shows an analysis of Ca^{2+} and Ba^{2+} blocking of ^{86}Rb influx in liposomes loaded with NaCl. It is clear that Ba^{2+} displays much stronger concentration dependent blocking of ^{86}Rb influx compared to Ca^{2+} (Fig. 4c).

Discussion

The four well defined ion binding sites in the NaK filter can be divided into three subtypes based on the nature of their ligands: carbonyl-water for the external site and vestibule, carbonyl-carbonyl for site 3, and carbonyl-hydroxyl for site 4. Despite their similar chemical

environments, these sites display a different ion binding preference as summarized in Table 1.

The external site, formed by 4 carbonyl oxygen atoms from Gly 67 along with extracellular water molecules can bind both mono (K^+ and Rb^+) and divalent (Ca^{2+} and Ba^{2+}) cations. Interestingly, no obvious Na^+ binding was observed at this site. This site is interesting in its apparently greater selectivity for divalent cations, which arises from the through space interaction between Asp66 and the Gly67-Asn68 peptide bond as reported previously [10].

With the involvement of four water molecules, the position of ion binding in the vestibule of the NaK selectivity filter is equivalent to that of site 2 in KcsA. However, the mobility of the water molecules imparts greater flexibility in ion binding, allowing the site to accommodate various monovalent cations (Na^+, K^+, Rb^+). Thus, even though the highly K^+ selective sites 1 & 2 of K^+ channels are absent, the channel is still equipped for optimal K^+ conduction through the use of water molecules that help create a ligand geometry similar to that in K^+ channel selectivity filters. These four water molecules have longer ion-water distances in the Na^+-complex than the K^+-complex and do not form an inner hydration shell around Na^+ ions. This might be a consequence of Na^+ having a much smaller radius than K^+ or Rb^+, and its preference for smaller hydration shells with 5∼6 water molecules [21, 22], which could spatially prevent an octahedral arrangement of ligands for Na^+ coordination.

Sites 3 and 4 in NaK are virtually identical to those in K^+ channels in terms of structure and ligand type as shown in the superimposition of their selectivity filter regions (Fig 5a). However, they exhibit vastly different ion binding properties. Site 3 in NaK is of particular interest as it appears to be the most non-selective, accommodating both mono- and divalent cations with wide ranging radii. The non-selective nature of this site also makes it inevitably susceptible to contamination from trace elements, leading to the presence of unknown species of ions at this site. Three major differences in ion binding at sites 3 and 4 between NaK and K^+ channels are obvious. First, Ba^{2+}, a well known K^+ channel blocker [23-26], binds at site 4 in K^+ channels but at site 3 in NaK. Second, Cs^+ can bind at both sites in K^+ channels but prefers to bind at site 3 in NaK in the presence of K^+. Finally, while Na^+ binds at both sites in NaK, no Na^+ binding was observed in K^+ channels. In light of no obvious structural differences in sites 3 and 4 between NaK and K^+ channels, these differences in Ba^{2+} and Cs^+ binding are intriguing and the underlying features that give rise to them require further investigation.

The unique ability of the NaK selectivity filter to utilize water molecules in sync with carbonyl oxygen atoms has important consequences for ion chelation. The ability to form octahedral ion chelation schemes seemingly makes the NaK selectivity filter more optimized for K^+ binding than Na^+. This hypothesis is supported by data from competition assays where externally added K^+ has a more pronounced effect on reducing ^{86}Rb accumulation in liposomes compared to Na^+ [11]. Theoretical studies of K^+ selectivity based on the KcsA structure have also suggested that an octahedral arrangement of oxygen ligands in the channel pore is more favorable for K^+ than Na^+([27-29]. However, this K^+ over Na^+ selectivity in NaK clearly does not occur to the same extent as in K^+ channels and NaK is able to conduct Na^+ well. Overall, we believe two factors may be key contributors to the ion

selectivity differences observed between NaK and K^+ channels. The first is the apparent need for K^+ ions to stabilize the selectivity filter of K^+ channels in the 'conducting' state. Replacement of K^+ with Na^+ leads to a 'collapsed' filter which yields the channel non conductive [30]. Such a dependence on K^+ ions for maintaining the structural integrity of the selectivity filter is not observed in the NaK channel, which maintains an almost identical structure in complex with Na^+, K^+, or Rb^+ as shown in figure 5b. It is worth noting that the presence of contaminating ions at site 3 makes it difficult to make any definitive assertions regarding subtle structural differences in the NaK selectivity filter. However, it is still clear that major rearrangements do not occur upon binding of different ions, as a mixture of proteins with two conformations at the filter region is not expected to yield well diffracting crystals. The structural stability of the NaK selectivity filter can be partly attributed to strong H-bonding interactions between Asp66 and the backbone amide of Asn68. Another cause could be related to how well Na^+ ions bind within the selectivity filter. In a recent study, mutation of a conserved Glycine (Gly77) residue to D-Ala in KcsA yielded a channel that maintained a conductive selectivity filter even in the presence of Na^+ [31]. The mutant channel can conduct Na^+ but is still very selective for K^+, suggesting that the 4 equivalent K^+ binding sites in a K^+ channel selectivity filter are not energetically favorable for Na^+ binding. The replacement of K^+ channel sites 1&2 with a water-filled vestibule in NaK may overcome this energy barrier and make Na^+ binding less unfavorable. Na^+ ions display versatility in relative positioning and number of ligands, as shown in the NaKN 19-Na^+ complex. Ions are not restricted to the middle of the ion binding sites, but bind at the upper and lower edges instead, in plane with 4 carbonyl or hydroxyl oxygen atoms. A well ordered water molecule in the cavity just below the selectivity filter participates in a pyramidal Na^+ chelation at site 4. This ligand geometry effectively reduces the ion-ligand distance and the coordination number of Na^+ to 2.4 Å and 5, respectively, consistent with the statistics of Na^+ coordination commonly observed in water, small molecules, or proteins [21, 32]. This planar configuration could very well be the case for a Na^+ ion at site 3 as the ion could be stabilized by a water molecule in the vestibule. Therefore, by having partial exposure to solvent, Na^+ can bind both at site 3 and 4 in a favorable planar configuration as also has been suggested in the recent computational studies of ion selectivity and conduction in NaK [13, 14].

Methods

Protein expression, purification, and crystallization

Detailed experimental procedures are described in our companion paper. Na^+, K^+, and Rb^+ complexes of NaKN 19 were purified with the corresponding salts (100 mM NaCl, KCl or RbCl) and crystallized over a well solution containing 55-70% (v/v)(±)-2-Methyl-2,4-pentanediol (MPD) and 100mM Hepes pH 7.5. All crystals used for the Ca^{2+} titration assay were obtained by using proteins purified in 100 mM NaCl and with the addition of 0.5-10mM $CaCl_2$ to the crystallization well solution. For soaking experiments, crystals of the NaKN 19-K^+ complex were soaked in stabilization solutions containing 67 mM KCl and 33 mM CsCl or $BaCl_2$ for one day.

A majority of the crystals suffered from either partial or perfect twinning [33]. Several data sets were therefore collected for each of the structures reported here and in our companion study to obtain at least one untwinned data set of high quality. The only exception was the data set collected for NaKND19-Rb$^+$ complex, which has a twinning fraction of 20% and was detwinned in CCP4 [34] before being used for refinement. All statistics of data collection and refinements are listed in Table 2.

One dimensional electron density profiles of external Ca^{2+} binding were obtained as described [35]. All data from Na$^+$ complexes co-crystallized with 0.5 – 10 mM Ca^{2+} were scaled to 2.1 Å using the native NaKND19-Na$^+$ crystal (without Ca^{2+}) as a reference. 1-D profiles were obtained by sampling the $F_{0.5\text{-}10mM\ Ca}$-$F_{0mM\ Ca}$ difference maps along the z/ central axis at the external site using MAPMAN [36]. Ion occupancy was obtained by integrating the area under each peak on the 1-D profile and normalizing it against that of the 10 mM Ca^{2+} peak.

[86]Rb Competition assays

The divalent cation (Ca^{2+} and Ba^{2+}) blockage of the NaK channel was studied by analyzing the competing effect of Ca^{2+} and Ba^{2+} in ^{86}Rb flux assay. In this competition assay, the tested ions (Ca^{2+} and Ba^{2+}) were added directly into the flux buffer at appropriate concentrations to give the desired final concentrations upon addition of liposomes. Ion flux was then allowed to proceed for 10 minutes before radioactivity levels were counted as described.

Coordinates

The atomic coordinates and structure factors of NaKN 19 have been deposited in the Protein Data Bank with accession numbers of 3E8H (K$^+$ complex), 3E8F (K$^+$/Ba^{2+} complex), 3E8B (Rb$^+$ complex), 3E89(100mM Na$^+$ complex,), 3E83 (500mM Na$^+$ complex), and 3E8G (100mM Na$^+$/10mM Ca^{2+} complex)

Supplementary Material

Refer to Web version on PubMed Central for supplementary material.

## Acknowledgments

References

1. Hille, B. Ion Channels of Excitable Membranes. 3rd. Sinauer Associates, Inc.; Sunderland, MA: 2001.

2. Long SB, et al. Atomic structure of a voltage-dependent K+ channel in a lipid membrane-like environment. Nature. 2007; 450(7168):376–82. [PubMed: 18004376]

3. Kuo A, et al. Crystal structure of the potassium channel KirBac1.1 in the closed state. Science. 2003; 300(5627):1922–6. [PubMed: 12738871]

4. Jiang Y, et al. The open pore conformation of potassium channels. Nature. 2002; 417(6888):523–6. [PubMed: 12037560]

5. Jiang Y, et al. X-ray structure of a voltage-dependent K+ channel. Nature. 2003; 423(6935):33–41. [PubMed: 12721618]

6. Long SB, Campbell EB, Mackinnon R. Crystal Structure of a Mammalian Voltage-Dependent Shaker Family K+ Channel. Science. 2005

7. Nishida M, et al. Crystal structure of a Kir3.1-prokaryotic Kir channel chimera. Embo J. 2007; 26(17):4005–15. [PubMed: 17703190]

8. Noskov SY, Berneche S, Roux B. Control of ion selectivity in potassium channels by electrostatic and dynamic properties of carbonyl ligands. Nature. 2004; 431(7010):830–4. [PubMed: 15483608]

9. Gouaux E, Mackinnon R. Principles of selective ion transport in channels and pumps. Science. 2005; 310(5753):1461–5. [PubMed: 16322449]

10. Alam A, Shi N, Jiang Y. Structural insight into Ca2+ specificity in tetrameric cation channels. Proc Natl Acad Sci U S A. 2007; 104(39):15334–9. [PubMed: 17878296]

11. Shi N, et al. Atomic structure of a Na+- and K+-conducting channel. Nature. 2006; 440(7083): 570–4. [PubMed: 16467789]

12. Phillips K, et al. The crystal structure of a parallel-stranded guanine tetraplex at 0.95 A resolution. J Mol Biol. 1997; 273(1):171–82. [PubMed: 9367755]

13. Vora T, Bisset D, Chung SH. Conduction of Na+ and K+ through the NaK channel: molecular and Brownian dynamics studies. Biophys J. 2008; 95(4):1600–11. [PubMed: 18456826]

14. Noskov SY, Roux B. Importance of hydration and dynamics on the selectivity of the KcsA and NaK channels. J Gen Physiol. 2007; 129(2):135–43. [PubMed: 17227917]

15. Zhou Y, et al. Chemistry of ion coordination and hydration revealed by a K+ channel-Fab complex at 2.0 A resolution. Nature. 2001; 414(6859):43–8. [PubMed: 11689936]

16. Katz AK, et al. Calcium Ion Coordination: A Comparison with That of Beryllium, Magnesium, and Zinc. J Am Chem Soc. 1996; 118(24):5752–5763.

17. Pidcock E, Moore GR. Structural characteristics of protein binding sites for calcium and lanthanide ions. J Biol Inorg Chem. 2001; 6(5-6):479–89. [PubMed: 11472012]

18. Lewit-Bentley A, Rety S. EF-hand calcium-binding proteins. Curr Opin Struct Biol. 2000; 10(6): 637–43. [PubMed: 11114499]

19. Jiang Y, MacKinnon R. The barium site in a potassium channel by x-ray crystallography. J Gen Physiol. 2000; 115(3):269–72. [PubMed: 10694255]

20. Lockless SW, Zhou M, MacKinnon R. Structural and thermodynamic properties of selective ion binding in a K+ channel. PLoS Biol. 2007; 5(5):e121. [PubMed: 17472437]

21. Varma S, Rempe SB. Coordination numbers of alkali metal ions in aqueous solutions. Biophys Chem. 2006; 124(3):192–9. [PubMed: 16875774]

22. Anan Tongaarm KRL, Rode Bernd M. Born-Oppenheimer ab Initio QM/MM Dynamics Simulations of Na+ and K+ in Water: From Structure Making to Structure Breaking Effects. J Phys Chem A. 1998; 102:10340–10347.

23. Neyton J, Miller C. Potassium blocks barium permeation through a calcium-activated potassium channel. J Gen Physiol. 1988; 92(5):549–67. [PubMed: 3235973]

24. Neyton J, Miller C. Discrete Ba2+ block as a probe of ion occupancy and pore structure in the high-conductance Ca2+ -activated K+ channel. J Gen Physiol. 1988; 92(5):569–86. [PubMed: 3235974]

25. Armstrong CM, Swenson RP Jr, Taylor SR. Block of squid axon K channels by internally and externally applied barium ions. J Gen Physiol. 1982; 80(5):663–82. [PubMed: 6294220]

26. Armstrong CM, Taylor SR. Interaction of barium ions with potassium channels in squid giant axons. Biophys J. 1980; 30(3):473–88. [PubMed: 6266531]

27. Varma S, Sabo D, Rempe SB. K+/Na+ selectivity in K channels and valinomycin: over-coordination versus cavity-size constraints. J Mol Biol. 2008; 376(1):13–22. [PubMed: 18155244]

28. Varma S, Rempe SB. Tuning ion coordination architectures to enable selective partitioning. Biophys J. 2007; 93(4):1093–9. [PubMed: 17513348]

29. Bostick DL, Brooks CL 3rd. Selectivity in K+ channels is due to topological control of the permeant ion's coordinated state. Proc Natl Acad Sci U S A. 2007; 104(22):9260–5. [PubMed: 17519335]

30. Zhou Y, MacKinnon R. The occupancy of ions in the K+ selectivity filter: charge balance and coupling of ion binding to a protein conformational change underlie high conduction rates. J Mol Biol. 2003; 333(5):965–75. [PubMed: 14583193]

31. Valiyaveetil FI, et al. Ion selectivity in a semisynthetic K+ channel locked in the conductive conformation. Science. 2006; 314(5801):1004–7. [PubMed: 17095703]

32. Harding MM. Metal-ligand geometry relevant to proteins and in proteins: sodium and potassium. Acta Crystallogr D Biol Crystallogr. 2002; 58(Pt 5):872–4. [PubMed: 11976508]

33. Yeates TO. Detecting and overcoming crystal twinning. Methods Enzymol. 1997; 276:344–58. [PubMed: 9048378]

34. Collaborative Computational Project, N. The CCP4 suite: programs for protein crystallography. Acta Crystallogr D Biol Crystallogr. 1994; 50:760–763. [PubMed: 15299374]

35. Morais-Cabral JH, Zhou Y, MacKinnon R. Energetic optimization of ion conduction rate by the K + selectivity filter. Nature. 2001; 414(6859):37–42. [PubMed: 11689935]

36. Kleywegt GJ, Jones TA. xdlMAPMAN and xdlDATAMAN - programs for reformatting, analysis and manipulation of biomacromolecular electron-density maps and reflection data sets. Acta Crystallogr D Biol Crystallogr. 1996; 52(Pt 4):826–8. [PubMed: 15299647]
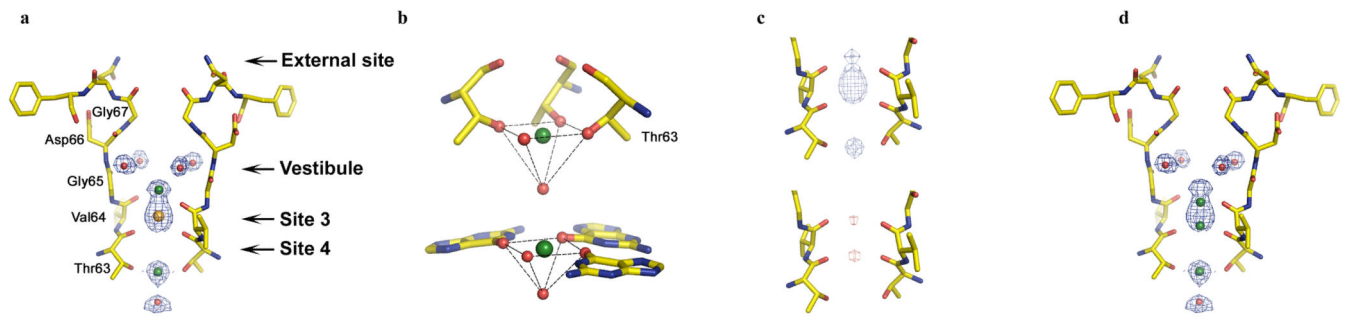
1.

Na$^+$ binding in the NaK filter (**a**) 2F$_o$-F$_c$ ion omit map contoured at 1.5σ showing density (blue mesh) for Na$^+$ ions, water molecules in the vestibule and central cavity, and the contaminating ion at site 3 (green, red, and orange spheres, respectively). The front and back subunits of the NaK model have been removed for clarity in most figures. (**b**) Comparison of Na$^+$ binding in NaK at site 4 (upper) and the 3′ side of the guanine tetraplex (lower) showing Na$^+$ binding in plane with 4 of its ligand, with a water molecule sitting axial to it. (**c**) 2F$_o$-F$_c$ ion omit map contoured at 2.5σ (blue mesh, upper) showing football shape of electron density at site 3 of NaKN 19 in high Na$^+$ (500mM); and the F$_o$-F$_c$ map with Cs$^+$ at site 3 contoured at 4 σ (red mesh, lower) showing density that likely arises from a contribution of Na$^+$ present on both the upper and lower edges of site 3. (**d**) Suggested mode of Na$^+$ binding at the upper and lower edges of site 3.
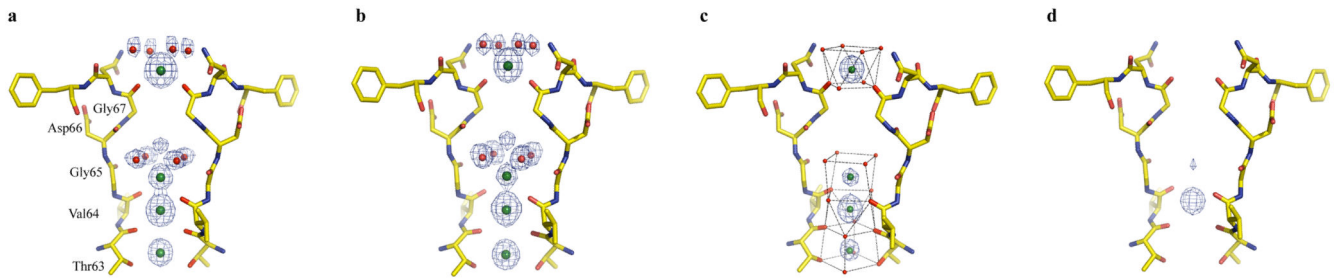
2.

K^+ and Rb^+ binding in the NaK selectivity filter. The $2F_o$-F_c ion omit maps (1.5σ) show electron density of ion binding in the K^+ complex (a) and Rb^+ complex **(b)** of NaKN 19. K^+ and Rb^+ ions are colored green with water molecules represented as red spheres. **c)** The maintenance of an octahedral ligand arrangement in the K^+ complex, which also holds true for the Rb^+ complex. Oxygen atoms from the front and back subunits chelating the ions are shown as red spheres. **d)** $F_{Cs\ soak} - F_K$ difference map contoured at 10 σ showing Cs^+ binding at site 3.
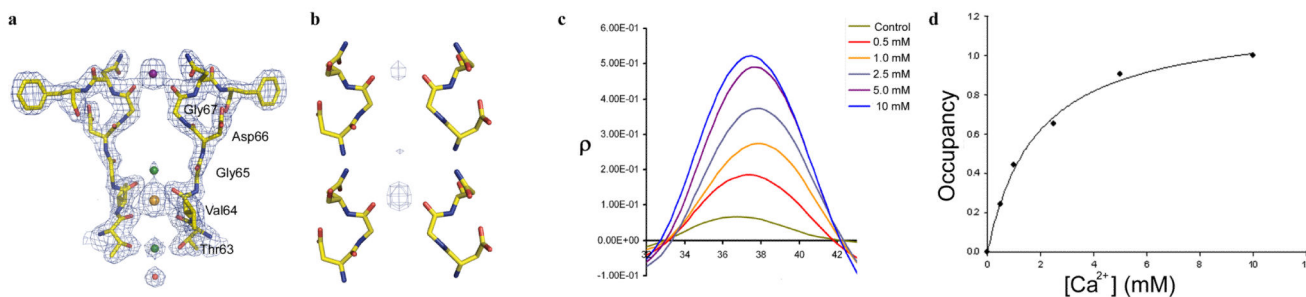
3.

Ca^{2+} binding in the NaK selectivity filter. **(a)** $2F_o$-F_c ion omit map (1.5σ) of the NaKN 19-Na^+ complex co-crystallized with 10mM $CaCl_2$, showing electron density for a Ca^{2+} ion (purple sphere) at the external entrance. Na^+ and the contaminant at site 3 are modeled as green and orange spheres, respectively. Electron density for the protein backbone is also shown as a blue mesh. **(b)** $F_{0.5mM\ Ca} - F_{0mM\ Ca}$ (upper) and $F_{5mM\ Ca^{2+}} - F_{0mM\ Ca^{2+}}$ (lower) difference map contoured at 10 σ showing increasing intensity of Ca^{2+} binding upon increasing Ca^{2+} concentration. Dotted lines indicate the position of central axis along which the 1-D electron density was calculated. **(c)** 1-D electron density profile of Ca^{2+} binding at the external entrance showing increased Ca^{2+} binding at increasing concentrations. The control is from a difference map between two native crystals grown in the absence of Ca^{2+}. **(d)** Occupancy of Ca^{2+} binding at the external site was calculated by integration of the peaks in 1-D electron density profile and normalizing them against the 10 mM Ca^{2+} peak. The plot of occupancy against Ca^{2+} concentration give rise to a K_d value of about 1.8 mM upon fitting the curve to a single component Langmuir equation.
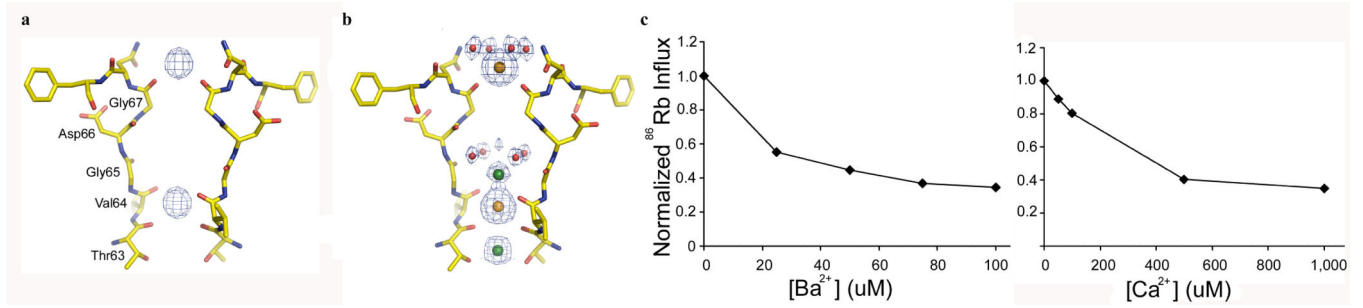
4.

Ba^{2+} binding in NaK filter. a) $F_{Ba\ soak} - F_K$ difference map (blue mesh) contoured at 10 σ showing the two Ba^{2+} binding sites. (b) $2F_o$-F_c ion omit maps of Ba^{2+}-soaked crystal contoured at 1.5 σ. The electron density at external entrance and site 3 was modeled as Ba^{2+} (orange spheres) and water molecules are modeled as red spheres. (c) Ba^{2+} (left) and Ca^{2+} (right) blocking of ^{86}Rb influx in liposomes loaded with NaCl.
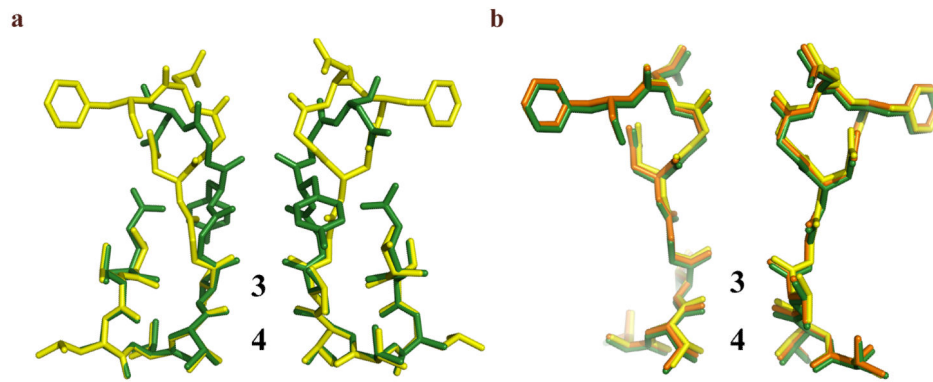
5.

Comparison of the selectivity filter structures of NaK and KcsA and between various ion complexes of NaK. **a)** Superimposition of the NaK selectivity filter (yellow) in complex with K$^+$ with that of KcsA (green, PDB code 1K4C). **b)** Superimposition of the selectivity filters of the NaKN 19 channel in complex with Na$^+$ (yellow), K$^+$ (green), and Rb$^+$ (orange).

Table 1

Ion Binding Properties of individual Sites In the NaK Selectivity Filter

Site	Ligand Type	Ion-ligand distance (Å)					Selectivity
		Na^+	K^+	Rb^+	Ba^{2+}	Ca^{2+}	
External	H_2O		3.06	2.77	2.94		K^+, Rb^+, Ca^{2+}, Ba^{2+}
	C=O (Gly67)		2.52	2.50	2.73	2.43	
Vestibule	H_2O	4.02	2.96	2.85			Na^+, K^+, Rb^+
	C=O (Val64)	2.94	3.00	3.11			
Site 3	C=O (Val64)		2.80	2.97			Na^+, K^+, Rb^+, Cs^+, Ca^{2+}, Ba^{2+}, others [*]
	C=O (Thr63)		2.83	2.94			
Site 4	C=O (Thr63)		2.97	2.98			Na^+, K^+, Rb^+
	-OH (Thr63)	2.38	2.79	2.89			

[*] refers to unknown contaminating ions.

Table 2

Data collection and refinement statistics for NaK N 19 in complex with various cations

NaK N 19-complex Conentrations (mM)	Na$^+$ 100	Na$^+$ 500	K$^+$ 100	Rb$^+$ 100	Na$^+$/Ca^{2+} 100/10	K$^+$/Ba^{2+} 67/33
Data collection						
Space group	I4	I4	I4	I4	I4	I4
Cell dimensions						
a=b(Å)	68.050	68.056	68.194	68.134	67.990	68.226
c (Å)	89.251	89.326	89.294	89.359	89.168	89.548
Resolution (Å)	50 - 1.8	50 - 1.8	50 - 1.8	50 - 1.7	50 - 2.0	50 - 2.0
R$_{sym}$ (%)	5.1 (65.5)	6.4 (82.1)	4.9 (56)	6.2 (59.9)	5.7 (34.3)	8.4 (60.4)
I/σI	36 (2)	30 (1.5)	41 (2)	31 (2)	38 (2.5)	26 (2.0)
Completeness (%)	99.3(99.3)	99.6(99.7)	99.6(99.6)	96.6(71.3)	97.2(81.6)	99.9(99.4)
Redundancy	6.8 (5.9)	6.8 (5.4)	7.0 (5.1)	6.8 (4.4)	6.6 (4.7)	6.9 (5.1)
Refinement						
Resolution (Å)	1.8.	1.8	1.8	1.7	2.0	2.0
No. Reflections	18808	18965	18948	21705	13398	13987
R$_{work}$ / R$_{free}$	21.3/24.8	21.5/23.6	21.2/23.4	22.0/22.9	20.0/23.5	20.1/24.8
No. atoms						
Protein	1462	1462	1462	1462	1462	1462
MPD / Ion	24/6	0/5	32/10	32/11	24/8	16/10
Water	144	111	96	94	52	57
B-factors						
Protein	37.60	36.06	34.692	30.583	49.385	39.206
Ligand/ion	49.03	30.592	50.317	51.79	67.043	51.841
Water	60.855	56.592	53.276	47.63	70.243	54.492
R.m.s.d						
Bond lengths (Å)	0.0060	0.0084	0.0053	0.0059	0.0062	0.0060
Bond angles (°)	1.089	1.260	1.070	1.116	1.099	1.068

*
Values in parentheses are for highest-resolution shell.